

Nematicity in LaFeAsO single crystals studied by elastoresistance, high-resolution thermal expansion and shear-modulus measurements

X. C. Hong^{‡, 1, 2, *} S. Sauerland,^{3, *} L. Wang,³ F. Scaravaggi,¹ A. U. B. Wolter,¹ R. Kappenberger,¹ S. Aswartham,¹ S. Wurmehl,¹ S. Sykora,¹ F. Caglieris,¹ B. Büchner,^{1, 4} C. Hess,^{1, 2} and R. Klingeler^{3, †}

¹*Leibniz-Institut für Festkörper u. Werkstofforschung (IFW) Dresden, Helmholtzstr. 20, 01069 Dresden, Germany*

²*Fakultät für Mathematik und Naturwissenschaften,
Bergische Universität Wuppertal, Gaußstraße 20, 42119 Wuppertal, Germany[‡]*

³*Kirchhoff Institute for Physics, Heidelberg University, D-69120 Heidelberg, Germany*

⁴*Institut für Theoretische Physik and Würzburg-Dresden Cluster of Excellence ct.qmat,
Technische Universität Dresden, 01062 Dresden, Germany*

(Dated: May 13, 2026)

Nematicity in LaFeAsO single crystals is studied by means of high-resolution thermal expansion, shear modulus, and elastoresistivity measurements. A softening of the shear modulus C_{66} towards the structural phase transition at T_S is observed. In addition, a similar Curie-Weiss-like divergence of the nematic susceptibilities is found in the temperature dependence of both χ^{sh} and χ^{er} , which are deduced from the shear modulus (sh) and the elastoresistivity (er) studies, respectively. These observations provide evidence for an electronic origin of nematicity in LaFeAsO. The characteristic energy of the coupling between the lattice and the electronic degrees of freedom is deduced to ~ 30 K. The comparison to corresponding measurements on BaFe₂As₂ single crystals reveals a very similar temperature dependence of the shear modulus but yields contrasting results for χ^{er} : In BaFe₂As₂, χ^{er} diverges similarly as the uncoupled nematicity deduced from the shear modulus data as it is expected from the underlying Landau theory. In contrast, the Weiss temperatures of χ^{er} and χ^{sh} are significantly different in LaFeAsO. This difference is at odds with the commonly anticipated theories of resistivity anisotropy and electronic nematicity in iron pnictides.

I. INTRODUCTION

Unconventional superconductivity is accompanied by a complex interplay of competing or intertwined degrees of freedom. The interaction responsible for Cooper pairing is usually believed to manifest itself as ordered phases or pertinent fluctuations in the stoichiometric parent compounds [1, 2]. In this context, electronic nematicity has been identified as an intriguing property that may enhance the superconducting transition temperature T_C [3–5]. While nematic fluctuations and/or nematic phases have been observed, e.g., in cuprate superconductors [6, 7] and other novel strongly correlated systems, the probably most prominent example is represented by iron-based superconductors (FeSC) [8, 9]. In most of their underdoped compounds, the tetragonal symmetry between the x - and y -directions in the Fe-plane is spontaneously broken when the system is cooled below its structural transition temperature T_S . The structural distortion is usually accompanied or followed by the evolution of long-range antiferromagnetic order T_N . In case of $T_N < T_S$, rotational C_4 -symmetry of the crystal lattice as well as the discrete Z_2 -symmetry lifting the degeneracy of the Ising-like electronic ground state are broken in the intermediate phase while time-reversal symmetry is still preserved. This intermediate phase is hence named nematic [5]. In this phase, electronic anisotropy is found to be impressively large compared to a rather small orthorhombic distortion which suggests that the structural-nematic transition does not arise from a simple elastic instability [10].

It is however challenging to determine the driving instability of nematicity since symmetry breaking affects all correlated degrees of freedom so that every elastic, electronic, spin, and orbital property becomes anisotropic at the structural-nematic phase transition. Studying the associated susceptibilities directly in the high-symmetry phase [11, 12] allows to disentangle their specific contributions. For example, the spontaneous elastic strain evolving at T_S as orthorhombic distortion δ acts as a conjugate field to a nematic order parameter ψ [5, 13] so that investigating the corresponding elastic and electronic response to an applied external stress σ by measurements of the elastoresistivity

* Both authors contributed equally.

† klingeler@kip.uni-heidelberg.de

‡ hongxc@cqu.edu.cn

and the elastic shear modulus have become powerful tools to access the nematic susceptibility [13–16].

$$\left(\frac{\partial\psi}{\partial\sigma}\right)^{-1} \propto \tilde{\chi}^{-1} = \chi^{-1} - C(\lambda). \quad (1)$$

In the literature [15, 17], χ is often referred to as bare or uncoupled nematic susceptibility whereas $\tilde{\chi}$ is termed renormalized or actual nematic susceptibility. Elastoresistivity measurements probe the normalized in-plane resistivity anisotropy $\eta = (\rho_b - \rho_a)/\rho_{\text{avg}}$ ¹, being a measure of the nematic order parameter, in dependence of strain ϵ . It thereby detects the purely electronic contribution to the nematic susceptibility, i.e., χ [13, 18]. On the other hand, the softening of the elastic shear modulus is directly associated with both $\tilde{\chi}$ and χ , which differ by a term $C(\lambda)$ which depends on the electron-lattice coupling λ . This term, to be discussed later, accounts for the reduction in the energy of the spontaneous orthorhombic distortion by nematic fluctuations via the electron-lattice coupling [5].

For BaFe₂As₂ and FeSe, the mentioned experiments have confirmed the shear modulus C_{66} as the elastic soft mode of the tetragonal-to-orthorhombic transition [14, 19–22], and have verified the transition’s electronic origin [13, 23–28]. However, the picture is yet incomplete as experimental results on ‘1111’-compounds are scarce. The relevance of such studies stems from the fact that, while FeSe does not show long-range magnetic order at ambient pressure and in undoped ‘122’-systems the structural-nematic and the magnetic phase transition coincide, in ‘1111’-compounds the transitions are split and give rise to another appearance of a nematic phase [29–31], presenting a unique testbed for intertwined orders. In addition, testing theoretical models of nematicity in this class of materials is also particularly relevant as the ‘1111’-family still holds the highest T_C among bulk FeSC at ambient pressure [32–34]. Previous experimental studies on LaFeAsO polycrystals showed clear indications of fluctuations of all relevant degrees of freedom well above T_S [35–38]. However, these investigations have so far been limited by constraints in single crystal growth. The recent developments in growing large high-quality single crystals [39] now enable detailed studies of the nematic properties in the ‘1111’-family of pnictides. Recent studies on single crystals show that nematic fluctuations promote spin fluctuations in magnetically ordered LaFeAsO [40] and foster the superconductivity in doped systems [41, 42]. In this paper, we present a combined study of elastoresistivity, high-resolution thermal expansion and shear modulus measurements in order to gain more insight into the microscopic origin of nematicity in LaFeAsO.

II. EXPERIMENTAL

Well-faceted LaFeAsO single crystals grown by the solid state single crystal growth (SSCG) method [39] of about $(1.0 \times 0.8 \times 0.3) \text{ mm}^3$ have been investigated. Thermal expansion studies were performed by means of a three-terminal high-resolution capacitance dilatometer (Kuechler Innovative Measurement Technology) in a home-built set-up [43, 44]. Temperature control was ensured by a Variable Temperature Insert of an Oxford magnet system [45]. The dilatometer’s built-in repulsion force of two leaf springs allows to detwin the sample for an orientation along the $[110]_t$ direction [43, 46]. The Young’s modulus along this particular direction has been obtained by a three-point-bending (3PB) technique similar as presented in Ref. [20]. In the dilatometer, a plate-like sample of about $(1.5 \times 1.5 \times 0.2) \text{ mm}^3$ is positioned between three rods as it is shown in the inset of Fig. 1(c). Thus, the force of the springs acting along the $[001]$ -direction bends the sample and its deflection is measured by the distance change of the dilatometer’s gap. This enables calculating Young’s modulus $Y_{[110]}$ which is directly related to the elastic constant C_{66} [47].

Single crystals from the same batch were used for elastoresistance measurements. Strain was generated by firmly gluing the prepared samples on the side of a piezoelectric actuator (PZT) [13]. The crystals were cut to rectangular shape with the long sides along the $[110]_t$ or $[100]_t$ directions. In order to achieve efficient strain transmission, the samples were cleaved to a thickness of around 20 μm . Electrical contacts were made directly on the fresh surfaces with silver paint. Resistance was measured by a standard four-point *dc* technique.

III. RESULTS

The thermal expansion data shown in Fig. 1(a) illustrate the temperature dependence of the lattice parameters, where b denotes the shorter in-plane direction of the detwinned crystal. The relative length changes along the a axis

¹ ρ_a and ρ_b are the resistivities along the tetragonal in-plane directions of the macroscopic sample; $\rho_{\text{avg}} = (\rho_a + \rho_b)/2$.

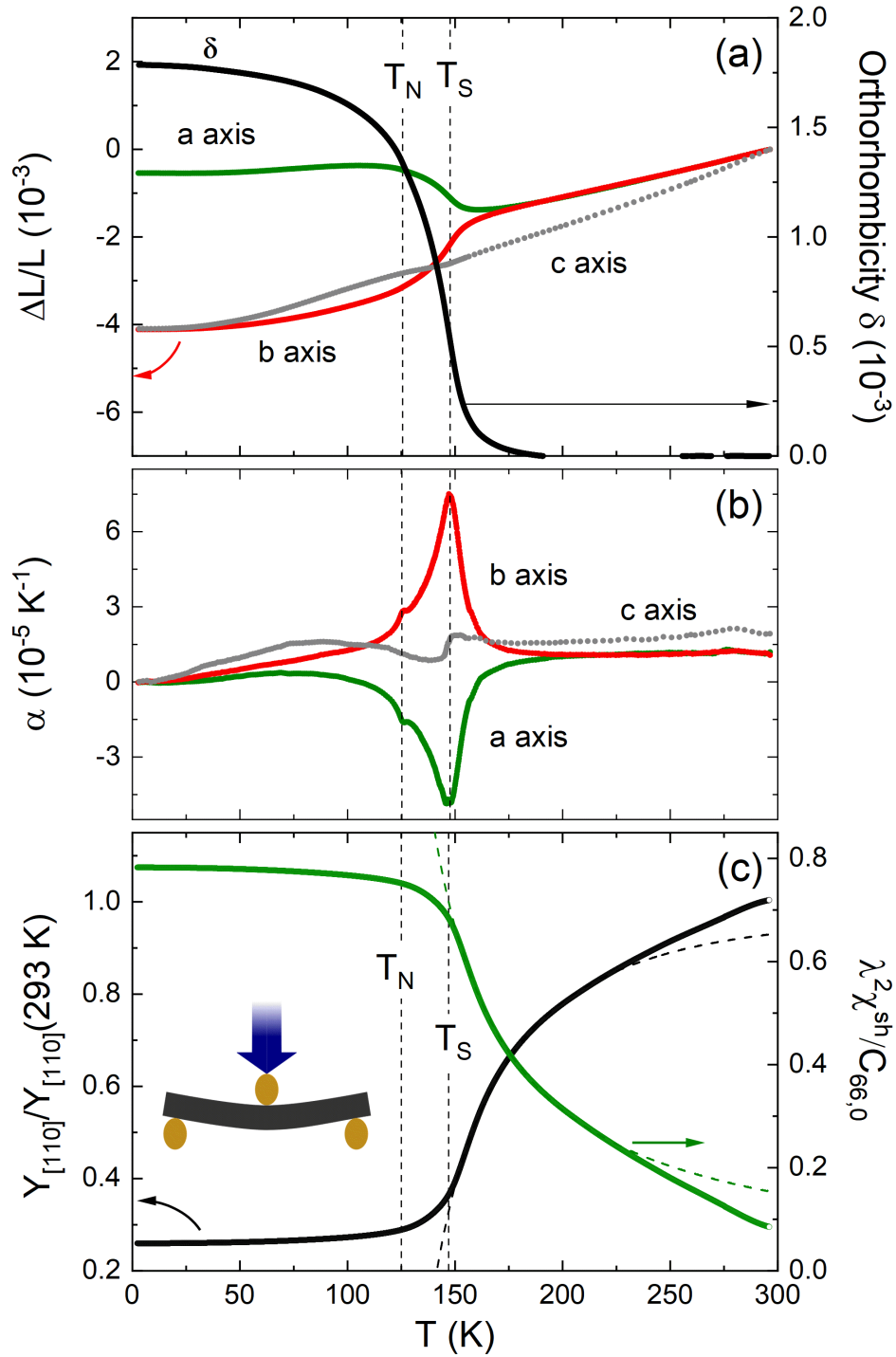


FIG. 1. (a) Relative length changes $\Delta L/L$ of the three main crystallographic axes (left scale) and orthorhombic distortion $\delta = (a - b)/(a + b)$ (right scale) vs. temperature. Structural and magnetic phase transition temperatures, T_S and T_N , of this crystal are marked by dashed lines. (b) Corresponding uniaxial thermal expansion coefficients. (c) Young's modulus $Y_{[110]_t}$ along the $[110]_t$ direction (left scale) and bare nematic susceptibility $\lambda^2 \chi^{sh}/C_{66,0}$ (right scale) together with Curie-Weiss fittings (dashed lines) according to Eq. 7. The inset shows a schematic sketch of the utilized 3PB-setup where the sample bends under an applied force (blue arrow).

have been calculated from the difference of length changes along the detwinned and the twinned $[100]_t$ direction (see Fig. A2 in the Appendix). While in the high-temperature tetragonal phase upon cooling, the sample shrinks along all three axes, the orthorhombic splitting of a and b signals the structural transition at $T_S = 148$ K. As shown in Fig. 1(a), an orthorhombic distortion $\delta = (a - b)/(a + b)$ evolves rather smoothly with a large precursor regime. The orthorhombic distortion δ represents the order parameter of the tetragonal-to-orthorhombic phase transition. Note that the evolution of orthorhombicity is affected by finite pressure applied in the experimental setup but the general behavior agrees well to neutron data [48] on polycrystalline $\text{LaFeAsO}_{1-x}\text{F}_x$ [49, 50].

The temperature dependence of Young's modulus $Y_{[110]}$, which above T_S probes the elastic shear modulus C_{66} , is depicted on the left ordinate in Fig. 1(c). Fairly similar to what has been observed in BaFe_2As_2 [20] and FeSe [22] (see also Fig. A1 in the Appendix), $Y_{[110]}$ shows a strong decrease towards T_S , thereby reflecting a clear softening of C_{66} . This implies that C_{66} is the soft mode of the orthorhombic distortion also in LaFeAsO . At T_S , the curve flattens in a rather continuous manner and the inflection point at 154.5 K marks a lower limit to observe the softening. Note, that inhomogeneous stress applied to the sample via the 3PB setup (see Fig. 1) may smear out the anomaly due to strong strain dependencies of T_S . Specifically, measurements under varying uniaxial pressure along the $[110]_t$ direction show a shift of T_S and, in BaFe_2As_2 , breaking of the C_4 -symmetry already above T_S [50–54]. We also note that, $Y_{[110]}(T_S)$ remains finite at T_S . This observation contrasts theory predictions of vanishing C_{66} but is typically observed in 3PB and in ultrasound experiments on BaFe_2As_2 [14, 20] and FeSe [21, 22]. Below T_S , $Y_{[110]}$ reaches a constant value which may be ascribed to the motion of structural domain walls in the orthorhombic phase [15, 55].

As shown in Fig. 1(a), the orthorhombic distortion parameter δ evolves continuously as similarly observed for LaFeAsO polycrystals [35, 48]. In addition, the temperature dependence of $Y_{[110]}$ and accordingly of C_{66} above T_S [see Fig. 1(c)] indicates that the structural transition is not barely driven by an elastic instability. In a proper ferroelastic scenario the shear modulus is supposed to decrease linearly with temperature [11] which is not observed in the data at hand.

The in-plane resistivity anisotropy η probes the nematic order parameter in dependence of elastic strain ϵ [13]

$$\chi^{er} = -d\eta/d\epsilon \propto -d\psi/d\epsilon. \quad (2)$$

Depending on the relative direction of the sample axis with respect to the strain direction, i.e., ϵ either $\parallel [110]_t$ or $\parallel [100]_t$, respectively, χ^{er} is related to the B_{2g} - or the B_{1g} -symmetry channel [18]. The experimental data shown in Fig. 2 indeed show strong differences for both channels. For $\epsilon \parallel [110]_t$, χ^{er} is large and diverges towards a kink at T_S while it is damped and featureless for $\epsilon \parallel [100]_t$. We conclude that the nematic order parameter only develops in the diagonal B_{2g} -channel which agrees with the shear modulus results as C_{66} refers to the same symmetry. This finding matches with those for other FeSC [17]. Note, the sign of χ^{er} is positive for LaFeAsO like in $\text{Ba}(\text{Fe}_{1-x}\text{Co}_x)_2\text{As}_2$ but χ^{er} is negative in FeSe [17, 23, 24]. The following discussion will focus on the data above T_S since the elastoresistance is known to be dominated by domain effects below T_S [10].

Similar to other FeSC [13, 15], the structural (and nematic) transition is described by means of a pseudo-proper ferroelastic approach where the free energy is given by

$$F = \frac{\chi^{-1}}{2} \psi^2 + \frac{C_0}{2} \epsilon^2 - \lambda \psi \epsilon - \sigma \epsilon. \quad (3)$$

In this Landau expansion, the electronic order parameter ψ is bilinearly coupled via λ to the elastic strain ϵ while σ refers to an externally applied stress. χ^{-1} stands for the inverse bare nematic susceptibility in absence of coupling while $C_0 (= C_{66,0})$ is the inverse bare elastic susceptibility that accounts for the elastic energy by $C_0 \epsilon^2/2$ in the absence of coupling. Minimizing the free energy with respect to ψ and ϵ reveals that the response of the nematic order parameter ψ to elastic strain ϵ is a direct measure of the uncoupled nematic susceptibility [13]

$$\left. \frac{d\psi}{d\epsilon} \right|_{\epsilon=0} = \lambda \chi. \quad (4)$$

Hence, the observed divergence of χ^{er} provides evidence for an electronic origin of nematicity in LaFeAsO .

Moreover, minimizing F yields that the shear modulus C_{66} is renormalized by the electron-lattice coupling with $\tilde{\chi}$ being the renormalized susceptibility [5, 15]:

$$C_{66} = \left(\frac{d\epsilon}{d\sigma} \right)^{-1} = C_0 \left(1 + \frac{\lambda^2 \tilde{\chi}}{C_0} \right)^{-1} = C_0 - \lambda^2 \chi. \quad (5)$$

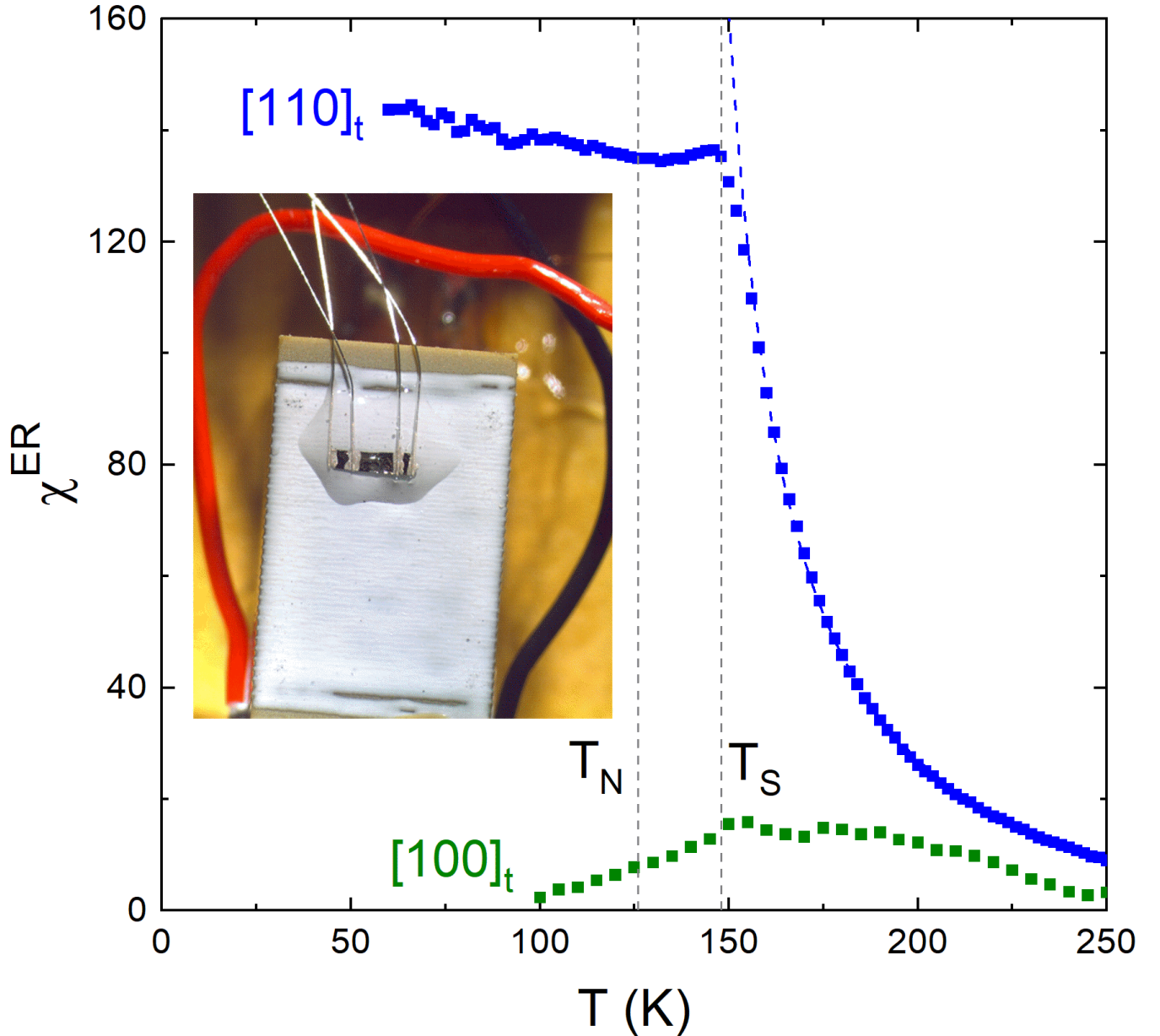


FIG. 2. Temperature dependence of the nematic susceptibility measured by elastoresistance $\chi^{er} = -d\eta/d\epsilon$. χ^{er} in the B_{2g} - and the B_{1g} -symmetry channels was investigated by applying strain ϵ along the $[110]_t$ and $[100]_t$ crystal directions, respectively. Dashed lines indicate T_S and T_N . The blue dashed line shows Curie-Weiss-fitting according to Eq. 8. The inset shows a photograph of a crystal glued on the surface of a PZT stack.

In case of finite electronic-elastic coupling λ , the structural phase transition hence appears at the temperature where the experimentally obtained inverse elastic susceptibility C_{66} as well as the inverse of the actual nematic susceptibility $\tilde{\chi}$ vanish [5, 15]. At this temperature, δ and ψ become finite although the nematic instability itself appears at lower temperature T_0 at which χ is expected to diverge [13]. Eq. 5 also demonstrates that the experimentally determined shear modulus C_{66} is directly linked to the renormalized nematic susceptibility $\tilde{\chi}$ and also the bare electronic contribution χ can be deduced [15].

Normalized values $Y/Y(293\text{ K})$ obtained by the 3PB-method [see Fig. 1(c), left scale] enable one to determine the uncoupled nematic susceptibility χ^{sh} in units of $\lambda^2/C_{66,0}$ using Eq. 5 and following Ref. [15], i.e.,

$$\lambda^2\chi^{sh}/C_{66,0} = 1 - C_{66}/C_{66,0} \approx 1 - Y_{[110]}/Y_0. \quad (6)$$

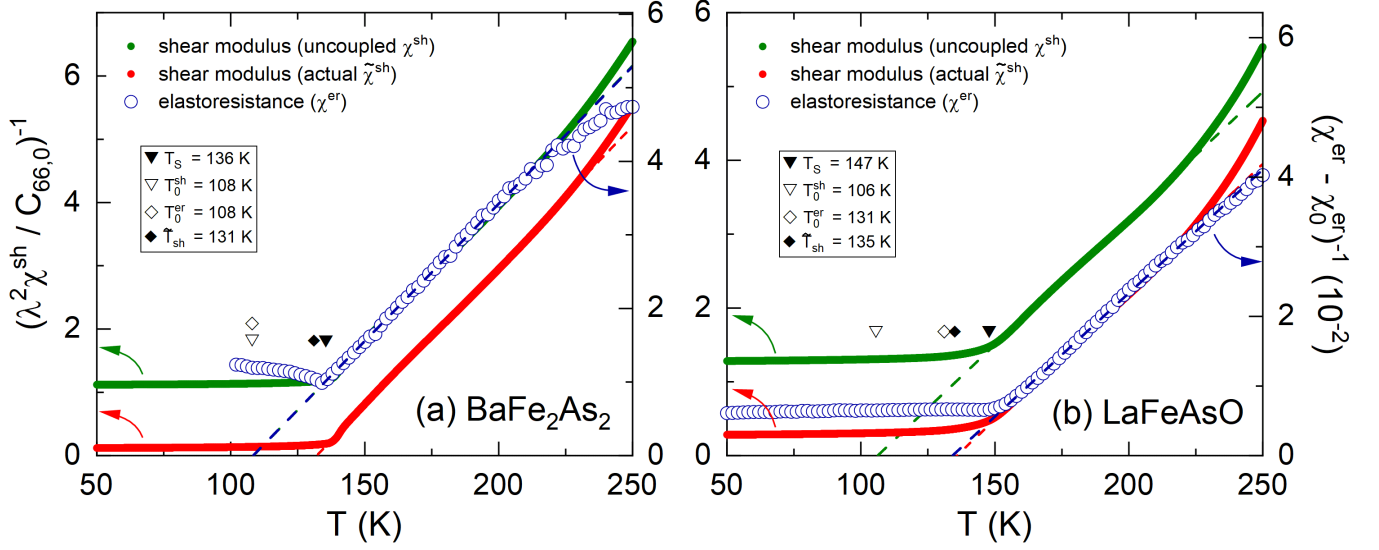


FIG. 3. Temperature dependence of the inverse purely electronic nematic susceptibilities $(\lambda^2 \chi^{sh} / C_{66,0})^{-1}$ (left scale, green markers) and $(\chi^{er} - \chi_0^{er})^{-1}$ (right scale, blue markers) of (a) BaFe₂As₂ and (b) LaFeAsO obtained by shear modulus and elasto-resistivity measurements, respectively. χ_0^{er} accounts for the intrinsic elasto-resistivity. In addition, $(\lambda^2 \tilde{\chi}^{sh} / C_{66,0})^{-1}$ (left scale, red markers) with the actual (renormalized) nematic susceptibility $\tilde{\chi}^{sh}$ is shown. The dashed lines represent Curie-Weiss fits to the data. Characteristic temperatures are indicated by grey markers (see the text).

Our treatment of the non-critical background $C_{66,0}$ and accordingly of Y_0 is based on the model for BaFe₂As₂ [20] using the formula by Y. P. Varshni [56] (denoted by F_{Varshni} in Eq. 7). The procedure involves the determination of a factor p^{sh} which links absolute values of the background and the present measurement and was also successfully applied for FeSe [22]. With the assumption $\chi^{-1} = a(T - T_0)$, usually utilized in Landau theories, Young's modulus data [Fig. 1(c), left scale] is well fitted by

$$\frac{Y_{[110]}}{Y_{[110]}(293 \text{ K})} = p^{sh} F_{\text{Varshni}} \left(1 - \frac{\lambda^2 / a C_{66,0}}{T - T_0^{sh}} \right). \quad (7)$$

The resulting uncoupled nematic susceptibility χ^{sh} is visualized in Fig. 1(c) (right scale). Similarly, the susceptibility χ^{er} from elasto-resistance is fitted by

$$\chi^{er} = \frac{p^{er} \lambda / a}{T - T_0^{er}} + \chi_0^{er} \quad (8)$$

where χ_0^{er} accounts for a background due to an intrinsic piezoresistivity and p^{er} for the unknown proportionality factor linking the strain dependence of the nematic order parameter ψ and the resistivity anisotropy η . Note the similar form of Eq. 7 and 8 which both contain three unknown fitting parameters.

In order to compare the critical behavior, the temperature dependencies of the inverse susceptibilities obtained from elasto-resistivity and shear modulus measurements are shown in Fig. 3(b), indicating a linear, i.e., Curie-Weiss-like decrease for both techniques in LaFeAsO. In Fig. 3(a), we additionally present the same quantities obtained in our experimental setups on BaFe₂As₂ single crystals [57, 58]. These data agree well with the previous literature [13, 17, 19, 20]. As expected from Landau theory, for BaFe₂As₂ we observe a linear, i.e., Curie-Weiss-like decrease upon cooling towards the nematic instability temperature T_0 . A fit to the data yields $T_0^{sh} = 108(6)$ K and $T_0^{er} = 108(5)$ K for the shear modulus and the elasto-resistivity data, respectively. We also show the actual, i.e., renormalized, nematic susceptibility $\tilde{\chi}^{sh}$ which is obtained from shear modulus data by Eq. 5. Obeying a Curie-Weiss-like behavior, $\tilde{\chi}^{sh}$ diverges at $\tilde{T}^{sh} = 131(3)$ K at which $Y_{[110]}$ extrapolates to zero according to Eq. 7. These results shown in Fig. 3 demonstrate a match of the bare mean field nematic critical temperatures obtained by two experimental techniques. Such a match was predicted by Landau theory but has not been explicitly reported in the literature so far [15, 17]. The behavior of χ^{er} , χ^{sh} , and $\tilde{\chi}^{sh}$ is further illustrated by scaling $(\chi^{er} - \chi_0^{er})^{-1}$ to $(\lambda^2 \chi^{sh} / C_{66,0})^{-1}$ by a single proportionality factor as it has been done by proper adjustment of the ordinates in Fig. 3. The scaling factor of about 0.009 may be attributed to the quantity $\lambda / p^{er} C_{66,0}$. Using literature data on χ^{er} [17] yields a very similar value.

For LaFeAsO, fitting χ^{sh} and $\tilde{\chi}^{sh}$ yield the Weiss temperatures $T_0^{sh} = 106(9)$ K and $\tilde{T}^{sh} = 135(3)$ K, respectively. These values are similar to those in BaFe₂As₂. Even the respective scaling factor p^{sh} is almost the same. In particular, normalizing the temperature axis to T_S of each material yields an almost identical decrease of $Y_{[110]}/Y_{[110]}(293\text{ K})$ for both compounds. So the main difference between BaFe₂As₂ and LaFeAsO lies in the discrepancy of the mean field (\tilde{T}^{sh}) and actual (T_S) structural transition temperature which is larger in LaFeAsO than in BaFe₂As₂ while the cause of this discrepancy, at all, is unknown [15]. From the difference $\tilde{T}^{sh} - T_0^{sh}$, we conclude that the characteristic energy scale of the coupling $\lambda^2/aC_{66,0}$ amounts to ~ 30 K [16]. This value is in accordance with the corresponding value for BaFe₂As₂ (see above) as well as the literature values for FeSe [22] and BaFe₂As₂ [20] and somewhat smaller than the one for BaFe₂As₂ reported in Ref. [19]. However, for the elastoresistance, the Curie-Weiss-analysis yields $T_0^{er} = 133(7)$ K which is significantly higher than T_0^{sh} . This difference cannot be explained by rationalization of experimental uncertainties since special care has been taken to account for the influence of the selected fitting temperature range and systematic correlations between fitting parameters due to the unknown backgrounds. Our analysis indicates, also for BaFe₂As₂, that fitting regimes closer to T_S tend to yield higher values for T_0^{sh} and \tilde{T}^{sh} but smaller ones for T_0^{er} . However, as visible by the uncertainties, this effect does not explain the large discrepancy for LaFeAsO.

In fact, T_0^{er} seems to match rather \tilde{T}^{sh} giving rise to scaling of $(\chi^{er} - \chi_0^{er})^{-1}$ and $(\lambda^2\tilde{\chi}^{sh}/C_{66,0})^{-1}$ by a factor of about 0.011 as shown in Fig. 3(c). So despite the differences of the Weiss temperatures, the corresponding Curie constants $p^{er}\lambda/a$ from elastoresistance as well as the ratio $\lambda/p^{er}C_{66,0}$ from the scaling are very similar for BaFe₂As₂ and LaFeAsO.

IV. DISCUSSION

Despite the strongly different appearance of a long-range magnetically ordered phase, the evolution of Young's modulus $Y_{[110]}$ and of the nematic susceptibility $\lambda^2\chi^{sh}/C_{66,0}$ [Fig. 1(c)] as well as of χ^{er} in the B_{2g} -channel (Fig. 2) imply clear similarities in LaFeAsO as compared to other FeSC such as BaFe₂As₂ [13, 20] and FeSe [22, 23]. Apparently, the absence of static nematic order in BaFe₂As₂ seems to have no significant impact on the softening of the shear modulus. A similar conclusion was drawn for FeSe where χ^{sh} almost resembles the behaviour of 3%Co-doped BaFe₂As₂ both exhibiting $T_S \sim 90$ K whereas FeSe does not show long-range magnetic order at finite temperatures at all [22].

Apart from these similarities, there is a clear discrepancy between the findings in LaFeAsO and BaFe₂As₂. In LaFeAsO, χ^{er} may be scaled to $\tilde{\chi}^{sh}$ rather than to χ^{sh} , i.e., the Weiss temperature $T_0^{er} = 133(7)$ K clearly exceeds T_0^{sh} but rather matches \tilde{T}^{sh} (cf. Fig. 3). This observation clearly contrasts the behaviour in BaFe₂As₂ as shown in Fig. 3(a) and the literature [17, 20].

Our results on LaFeAsO may be also compared to Co-doped Ba(Fe_{1-x}Co_x)₂As₂ which, for $x \neq 0$, exhibits a static nematic phase, i.e., $T_S > T_N$. While for $x = 0$ and 0.025, Kuo *et al.* [17] determined T_0^{er} from elastoresistivity to be well below \tilde{T}^{sh} observed by shear modulus measurements [20], T_0^{er} appears to be even larger than \tilde{T}^{sh} for higher doping ($x=0.047$). As a potential reason, an overestimation of T_0^{er} in fitting due to low temperature deviations from Curie-Weiss behavior observed in these compounds has been suggested [15]. However, our data of both techniques and for both compounds emphasize a very clear Curie-Weiss behavior even down to temperatures close to T_S giving no indication for physics beyond a mean-field approach.

Moreover, Curie constants from elastoresistivity are nearly the same for BaFe₂As₂ and LaFeAsO so that the data do not show any significant enhancement of χ^{er} for one of the compounds. Such an enhancement of the elastoresistivity has been observed in Ba(Fe,Co)₂As₂ upon approaching optimal doping and has been associated with renormalization of the quasiparticle effective mass by nematic quantum critical fluctuations [17]. However, we cannot exclude that the proximity of a quantum critical point causes the unexpectedly high T_0^{er} . In this case, our data would suggest an enhancement of the elastoresistance in LaFeAsO already far below the superconducting regime placing LaFeAsO closer to quantum criticality than BaFe₂As₂. Apart from that, it is not fully understood how magnetic and orbital fluctuations microscopically influence the elastoresistivity and shear modulus. Such effects might differ for transport and thermodynamic properties. In this respect, χ^{er} is thought to be influenced by the detailed electronic structure and/or scattering processes [17, 23, 24].

Therefore, especially the effect of disorder as a possible explanation for the resistivity anisotropy has already been widely addressed in the literature, both experimentally and theoretically [51, 59–64]. In particular, Kuo and Fisher argued that for undoped as well as for Co- and Ni-underdoped BaFe₂As₂, the evolution of the nematic susceptibility and the resulting Weiss temperatures T_0^{er} are essentially independent of disorder [65]. Moreover, the magnitude of the elastoresistance coefficient is found to be similar for all optimally doped BaFe₂As₂ compounds, suggesting that disorder

emerging from different types of dopants is not at play [17]. Related to this, our data for BaFe_2As_2 and LaFeAsO indicate no significant difference between their respective Curie constants $p^{\text{er}}\lambda/a$ from elastoresistivity. On the other hand, Gastiasoro *et al.* [62] suggested that assuming a significant amount of disorder in the samples, anisotropic spin fluctuations provoked by orthorhombic symmetry breaking are locally pinned to impurities and, thereby, establish defect states called nematogens. By this, the defects exhibit anisotropic scattering potentials which hence manifest themselves in an anisotropic resistivity. Calculations [66] based on this model may even reproduce a Curie-Weiss-like divergence of $d\psi/d\delta$ (δ : orbital order parameter accounting for orthorhombicity of the band dispersion) towards the bare magnetic phase transition temperature $T_{\text{N},0}$. In Ref. [62], the authors are in particular pointing out that Kuo's investigations [65] would rather refer to out-of-plane disorder and within the mentioned scenario, the anisotropy is mostly caused by spin fluctuations so that different kinds of impurities should be reflected rather in the average resistivity than its anisotropy. Within the scenario of disorder, our findings would propose a larger effect of disorder in LaFeAsO than in BaFe_2As_2 which is consistent with expectations for systems that show split second-order nematic and magnetic transitions as in LaFeAsO and underdoped $\text{Ba}(\text{Fe},\text{Co})_2\text{As}_2$ compared to simultaneous (or close-by) transitions as in BaFe_2As_2 [12]. Recent experimental investigations on optimally doped $\text{LaFeAsO}_{1-x}\text{F}_x$ polycrystals emphasize the high sensitivity of these compounds on magnetic impurities where already 0.5% Mn/Fe substitution re-establishes a magnetically ordered, orthorhombic state similar as it appears in undoped LaFeAsO [67–69]. Strong electronic correlations have been suggested to provoke enhanced RKKY-coupling between Mn defects and thereby localization of electrons [69, 70].

From a different perspective, also stoichiometry of the samples may affect the transport properties. While Ba122-systems are rather stoichiometric, 1111-systems are known to possibly exhibit oxygen deficiencies [71] which are discussed for single crystals of the present work [39] as a possible explanation for lower values of T_{S} and T_{N} compared to the respective values of polycrystals.

However, more experimental research as well as theoretical calculations are needed to clarify the importance and the role of disorder. Our study, therefore, indicates a good starting point for such a study opening up that the direct comparison of shear modulus and elastoresistivity on the doping evolution of LaFeAsO single crystals might shed more light on these open questions.

V. SUMMARY

We report measurements of the thermal expansion, the shear modulus, and the elastoresistivity in order to investigate the nematic phase in LaFeAsO single crystals. Our data imply a clear softening of the shear modulus C_{66} towards the structural phase transition at T_{S} and a similar Curie-Weiss-like divergence of the nematic susceptibility obtained with both techniques, i.e., shear modulus and elastoresistivity studies. We therefore conclude an electronic origin of nematicity in LaFeAsO . A characteristic energy scale of ~ 30 K for the electron-lattice coupling λ^2/aC_0 is obtained. The softening of C_{66} does not show any significant difference between LaFeAsO and the iconic BaFe_2As_2 when accounting for their different T_{S} , albeit the emergence of their corresponding nematic phase is significantly different. The Curie-Weiss-like divergence of the purely electronic nematic susceptibility probed by elastoresistivity in BaFe_2As_2 and LaFeAsO , however, indicates a significant difference in both materials. In BaFe_2As_2 , the mean-field divergence of χ occurs at a temperature consistent with the corresponding temperature determined from shear modulus data. While this is expected from the Landau theory, in LaFeAsO this divergence in χ appears at a significantly higher temperature than in the shear modulus data. Specifically, the critical part of the susceptibility measured by elastoresistivity scales to the renormalized nematic susceptibility obtained from shear modulus' softening. This observation challenges present theories of resistivity anisotropy and electronic nematicity in iron pnictides.

Our results extend the current picture of the family of iron-based superconductors revealing that LaFeAsO as representative for the '1111'-type compounds shows a softening of the shear modulus similar to what has been observed in '122'- [14, 20] and '11'- [22] compounds. Thereby, adding our results for the '1111'-system make the observed softening of the shear modulus an ubiquitous property of iron-based superconductors. Stark qualitative differences of the behaviour in LaFeAsO to the observations in the other pnictide families however pose new questions on the elastoresistivity, calling for further theoretical investigation.

ACKNOWLEDGMENTS

We thank C. Meingast and A. Böhmer for valuable discussions. Support by Deutsche Forschungsgemeinschaft (DFG) under Germany's Excellence Strategy EXC2181/1-390900948 (the Heidelberg STRUCTURES Excellence Cluster)

as well as through the Priority Programme SPP1458 via grant no. KL1827/6-1 is gratefully acknowledged. L.W. acknowledges funding through grants no. WA4313/1-1&2.

APPENDIX

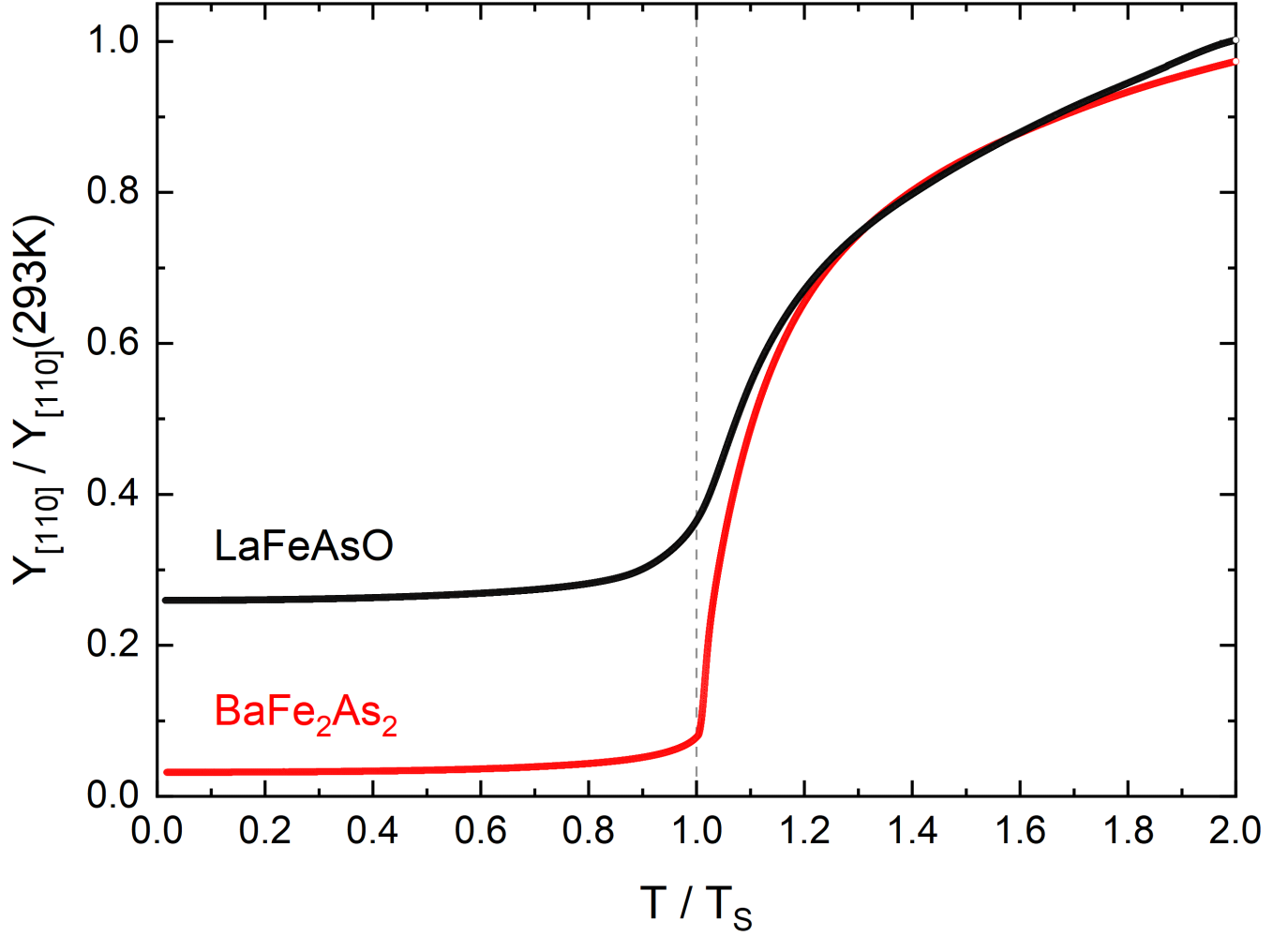


FIG. A1. Normalized Young's modulus in LaFeAsO and BaFe₂As₂ vs. temperature scaled to the respective structural transition temperature T_S .

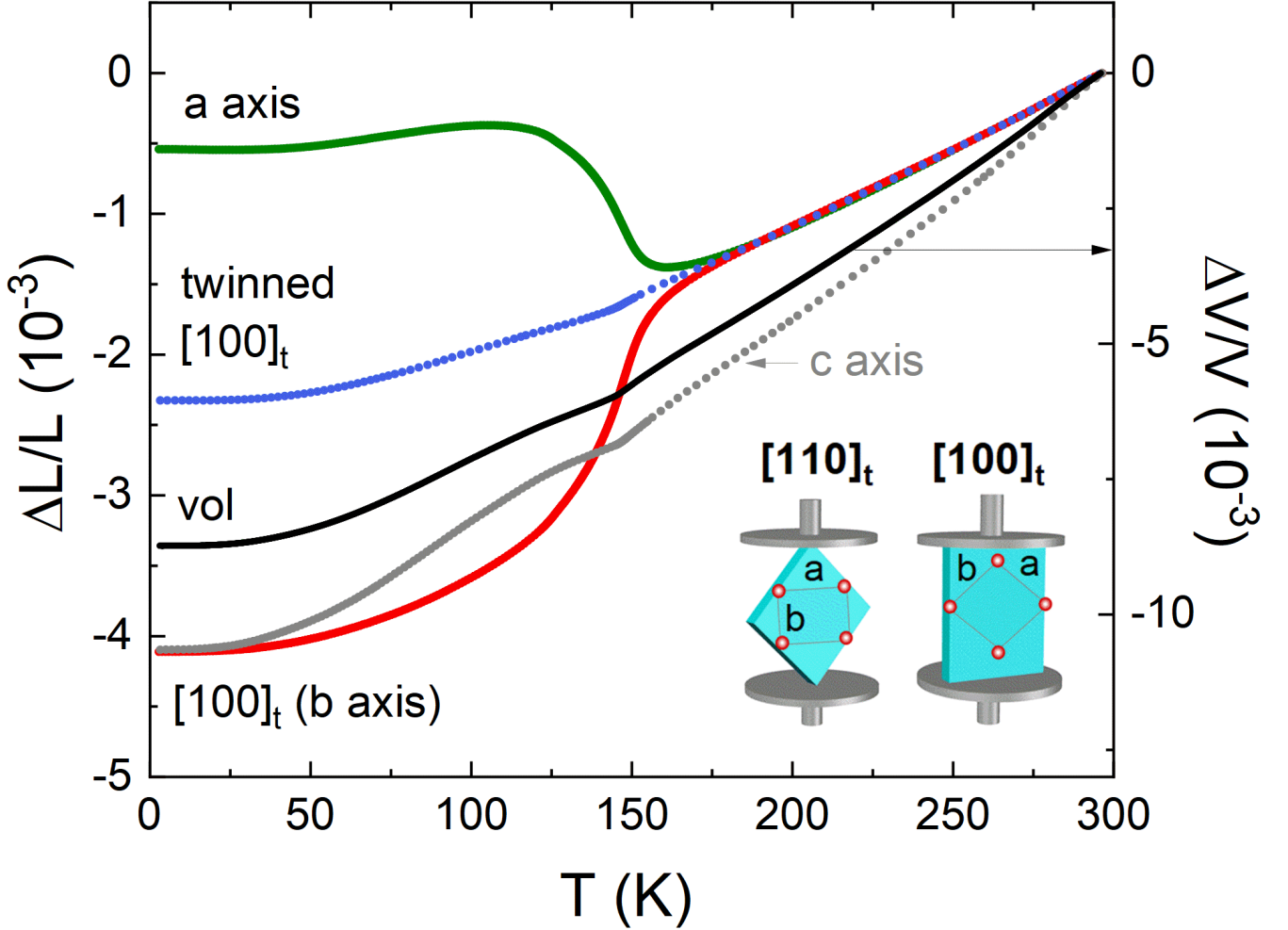


FIG. A2. Relative length changes $\Delta L/L$ of the three main crystallographic axes and as measured along the twinned $[100]_t$ direction as well as the resultant calculated volume changes $\Delta V/V$. The inset schematically illustrates the measurements along the twinned and detwinned in-plane directions from which the a axis length changes are obtained.

-
- [1] A. Chubukov, Pairing mechanism in Fe-Based superconductors, *Annual Review of Condensed Matter Physics* **3**, 57–92 (2012).
 - [2] P. J. Hirschfeld, M. M. Korshunov, and I. I. Mazin, Gap symmetry and structure of Fe-based superconductors, *Reports on Progress in Physics* **74**, 124508 (2011).
 - [3] E. Fradkin, S. A. Kivelson, M. J. Lawler, J. P. Eisenstein, and A. P. Mackenzie, Nematic Fermi fluids in condensed matter physics, *Annual Review of Condensed Matter Physics* **1**, 153–178 (2010).
 - [4] S. Lederer, Y. Schattner, E. Berg, and S. Kivelson, Enhancement of superconductivity near a nematic quantum critical point, *Physical Review Letters* **114**, 10.1103/physrevlett.114.097001 (2015).
 - [5] R. M. Fernandes and J. Schmalian, Manifestations of nematic degrees of freedom in the magnetic, elastic, and superconducting properties of the iron pnictides, *Superconductor Science and Technology* **25**, 084005 (2012).
 - [6] M. J. Lawler, K. Fujita, J. Lee, A. R. Schmidt, Y. Kohsaka, C. K. Kim, H. Eisaki, S. Uchida, J. C. Davis, J. P. Sethna, and E.-A. Kim, Intra-unit-cell electronic nematicity of the high- T_C copper-oxide pseudogap states, *Nature* **466**, 347–351 (2010).
 - [7] B. Keimer, S. A. Kivelson, M. R. Norman, S. Uchida, and J. Zaanen, From quantum matter to high-temperature superconductivity in copper oxides, *Nature* **518**, 179–186 (2015).
 - [8] D. C. Johnston, The puzzle of high temperature superconductivity in layered iron pnictides and chalcogenides, *Advances*

- in *Physics* **59**, 803–1061 (2010).
- [9] G. R. Stewart, Superconductivity in iron compounds, *Reviews of Modern Physics* **83**, 1589–1652 (2011).
 - [10] I. R. Fisher, L. Degiorgi, and Z. X. Shen, In-plane electronic anisotropy of underdoped ‘122’ Fe-arsenide superconductors revealed by measurements of detwinned single crystals, *Reports on Progress in Physics* **74**, 124506 (2011).
 - [11] A. Cano, M. Civelli, I. Eremin, and I. Paul, Interplay of magnetic and structural transitions in iron-based pnictide superconductors, *Physical Review B* **82**, 10.1103/physrevb.82.020408 (2010).
 - [12] R. M. Fernandes, A. V. Chubukov, and J. Schmalian, What drives nematic order in iron-based superconductors?, *Nature Physics* **10**, 97–104 (2014).
 - [13] J.-H. Chu, H.-H. Kuo, J. G. Analytis, and I. R. Fisher, Divergent nematic susceptibility in an iron arsenide superconductor, *Science* **337**, 710–712 (2012).
 - [14] R. M. Fernandes, L. H. VanBebber, S. Bhattacharya, P. Chandra, V. Keppens, D. Mandrus, M. A. McGuire, B. C. Sales, A. S. Sefat, and J. Schmalian, Effects of nematic fluctuations on the elastic properties of iron arsenide superconductors, *Physical Review Letters* **105**, 10.1103/physrevlett.105.157003 (2010).
 - [15] A. E. Böhmer and C. Meingast, Electronic nematic susceptibility of iron-based superconductors, *Comptes Rendus. Physique* **17**, 90–112 (2015).
 - [16] A. E. Böhmer, J.-H. Chu, S. Lederer, and M. Yi, Nematicity and nematic fluctuations in iron-based superconductors, *Nature Physics* **18**, 1412–1419 (2022).
 - [17] H.-H. Kuo, J.-H. Chu, J. C. Palmstrom, S. A. Kivelson, and I. R. Fisher, Ubiquitous signatures of nematic quantum criticality in optimally doped Fe-based superconductors, *Science* **352**, 958–962 (2016).
 - [18] H.-H. Kuo, M. C. Shapiro, S. C. Riggs, and I. R. Fisher, Measurement of the elastoresistivity coefficients of the underdoped iron arsenide $\text{Ba}(\text{Fe}_{0.975}\text{Co}_{0.025})_2\text{As}_2$, *Physical Review B* **88**, 10.1103/physrevb.88.085113 (2013).
 - [19] M. Yoshizawa, D. Kimura, T. Chiba, S. Simayi, Y. Nakanishi, K. Kihou, C.-H. Lee, A. Iyo, H. Eisaki, M. Nakajima, and S.-I. Uchida, Structural quantum criticality and superconductivity in iron-based superconductor $\text{Ba}(\text{Fe}_{1-x}\text{Co}_x)_2\text{As}_2$, *Journal of the Physical Society of Japan* **81**, 024604 (2012).
 - [20] A. E. Böhmer, P. Burger, F. Hardy, T. Wolf, P. Schweiss, R. Fromknecht, M. Reinecker, W. Schranz, and C. Meingast, Nematic susceptibility of hole-doped and electron-doped BaFe_2As_2 iron-based superconductors from shear modulus measurements, *Physical Review Letters* **112**, 10.1103/physrevlett.112.047001 (2014).
 - [21] G. A. Zvyagina, T. N. Gaydamak, K. R. Zhekov, I. V. Bilich, V. D. Fil, D. A. Chareev, and A. N. Vasiliev, Acoustic characteristics of FeSe single crystals, *EPL (Europhysics Letters)* **101**, 56005 (2013).
 - [22] A. Böhmer, T. Arai, F. Hardy, T. Hattori, T. Iye, T. Wolf, H. Löhneysen, K. Ishida, and C. Meingast, Origin of the tetragonal-to-orthorhombic phase transition in FeSe: A combined thermodynamic and NMR study of nematicity, *Physical Review Letters* **114**, 10.1103/physrevlett.114.027001 (2015).
 - [23] S. Hosoi, K. Matsuura, K. Ishida, H. Wang, Y. Mizukami, T. Watashige, S. Kasahara, Y. Matsuda, and T. Shibauchi, Nematic quantum critical point without magnetism in $\text{FeSe}_{1-x}\text{S}_x$ superconductors, *Proceedings of the National Academy of Sciences* **113**, 8139–8143 (2016).
 - [24] M. A. Tanatar, A. E. Böhmer, E. Timmons, M. Schütt, G. Drachuck, V. Taufour, K. Kothapalli, A. Kreyssig, S. Bud’ko, P. Canfield, R. Fernandes, and R. Prozorov, Origin of the resistivity anisotropy in the nematic phase of FeSe, *Physical Review Letters* **117**, 10.1103/physrevlett.117.127001 (2016).
 - [25] M. D. Watson, T. K. Kim, A. A. Haghhighirad, N. R. Davies, A. McCollam, A. Narayanan, S. F. Blake, Y. L. Chen, S. Ghannadzadeh, A. J. Schofield, M. Hoesch, C. Meingast, T. Wolf, and A. I. Coldea, Emergence of the nematic electronic state in FeSe, *Physical Review B* **91**, 10.1103/physrevb.91.155106 (2015).
 - [26] S.-H. Baek, D. V. Efremov, J. M. Ok, J. S. Kim, J. van den Brink, and B. Büchner, Orbital-driven nematicity in FeSe, *Nat. Mater.* **14**, 210 (2015).
 - [27] A. Fedorov, A. Yaresko, T. K. Kim, Y. Kushnirenko, E. Haubold, T. Wolf, M. Hoesch, A. Grüneis, B. Büchner, and S. V. Borisenko, Effect of nematic ordering on electronic structure of FeSe, *Sci. Rep.* **6** (2016).
 - [28] S.-H. Baek, J. M. Ok, J. S. Kim, S. Aswartham, I. Morozov, D. Chareev, T. Urata, K. Tanigaki, Y. Tanabe, B. Büchner, and D. V. Efremov, Separate tuning of nematicity and spin fluctuations to unravel the origin of superconductivity in FeSe, *Npj Quantum Mater.* **5** (2020).
 - [29] C. de la Cruz, Q. Huang, J. W. Lynn, J. Li, W. R. II, J. L. Zarestky, H. A. Mook, G. F. Chen, J. L. Luo, N. L. Wang, and P. Dai, Magnetic order close to superconductivity in the iron-based layered $\text{LaO}_{1-x}\text{F}_x\text{FeAs}$ systems, *Nature* **453**, 899–902 (2008).
 - [30] H. Luetkens, H.-H. Klauss, M. Kraken, F. J. Litterst, T. Dellmann, R. Klingeler, C. Hess, R. Khasanov, A. Amato, C. Baines, M. Kosmala, O. J. Schumann, M. Braden, J. Hamann-Borrero, N. Leps, A. Kondrat, G. Behr, J. Werner, and B. Büchner, The electronic phase diagram of the $\text{LaO}_{1-x}\text{F}_x\text{FeAs}$ superconductor, *Nature Materials* **8**, 305–309 (2009).
 - [31] C. Hess, H. Grafe, A. Kondrat, G. Lang, F. Hammerath, L. Wang, R. Klingeler, G. Behr, and B. Büchner, Nematicity in $\text{LaFeAsO}_{1-x}\text{F}_x$, *physica status solidi (b)* **254**, 10.1002/pssb.201600214 (2016).
 - [32] C. Wang, L. Li, S. Chi, Z. Zhu, Z. Ren, Y. Li, Y. Wang, X. Lin, Y. Luo, S. Jiang, X. Xu, G. Cao, and Z. Xu, Thorium-doping-induced superconductivity up to 56 K in $\text{Gd}_{1-x}\text{Th}_x\text{FeAsO}$, *EPL (Europhysics Letters)* **83**, 67006 (2008).
 - [33] G. Wu, Y. L. Xie, H. Chen, M. Zhong, R. H. Liu, B. C. Shi, Q. J. Li, X. F. Wang, T. Wu, Y. J. Yan, J. J. Ying, and X. H. Chen, Superconductivity at 56 K in samarium-doped SrFeAsF , *Journal of Physics: Condensed Matter* **21**, 142203 (2009).
 - [34] P. Cheng, B. Shen, G. Mu, X. Zhu, F. Han, B. Zeng, and H.-H. Wen, High- T_c superconductivity induced by doping rare-earth elements into CaFeAsF , *EPL (Europhysics Letters)* **85**, 67003 (2009).
 - [35] L. Wang, U. Köhler, N. Leps, A. Kondrat, M. Nale, A. Gasparini, A. de Visser, G. Behr, C. Hess, R. Klingeler, and B. Büchner, Thermal expansion of LaFeAsOF : Evidence for high-temperature fluctuations, *Physical Review B* **80**,

- 10.1103/physrevb.80.094512 (2009).
- [36] H.-J. Grafe, G. Lang, F. Hammerath, D. Paar, K. Manthey, K. Koch, H. Rosner, N. J. Curro, G. Behr, J. Werner, N. Leps, R. Klingeler, H.-H. Klauss, F. J. Litterst, and B. Büchner, Electronic properties of $\text{LaO}_{1-x}\text{F}_x\text{FeAs}$ in the normal state probed by NMR/NQR, *New Journal of Physics* **11**, 035002 (2009).
- [37] H. Maeter, H. Luetkens, Y. G. Pashkevich, A. Kwadrin, R. Khasanov, A. Amato, A. A. Gusev, K. V. Lamonova, D. A. Chervinskii, R. Klingeler, C. Hess, G. Behr, B. Büchner, and H.-H. Klauss, Interplay of rare earth and iron magnetism in $R\text{FeAsO}$ ($R = \text{La, Ce, Pr, and Sm}$): Muon-spin relaxation study and symmetry analysis, *Phys. Rev. B* **80**, 094524 (2009).
- [38] R. Klingeler, N. Leps, I. Hellmann, A. Popa, U. Stockert, C. Hess, V. Kataev, H.-J. Grafe, F. Hammerath, G. Lang, S. Wurmehl, G. Behr, L. Harnagea, S. Singh, and B. Büchner, Local antiferromagnetic correlations in the iron pnictide superconductors $\text{LaFeAsO}_{1-x}\text{F}_x$ and $\text{Ca}(\text{Fe}_{1-x}\text{Co}_x)_2\text{As}_2$ as seen via normal-state susceptibility, *Phys. Rev. B* **81**, 024506 (2010).
- [39] R. Kappenberger, S. Aswartham, F. Scaravaggi, C. G. Blum, M. I. Sturza, A. U. Wolter, S. Wurmehl, and B. Büchner, Solid state single crystal growth of three-dimensional faceted LaFeAsO crystals, *Journal of Crystal Growth* **483**, 9 (2018).
- [40] J. M. Ok, S.-H. Baek, D. V. Efremov, R. Kappenberger, S. Aswartham, J. S. Kim, J. van den Brink, and B. Büchner, Nematicity and magnetism in LaFeAsO single crystals probed by ^{75}As nuclear magnetic resonance, *Phys. Rev. B* **97**, 180405 (2018).
- [41] X. Hong, F. Caglieris, R. Kappenberger, S. Wurmehl, S. Aswartham, F. Scaravaggi, P. Lepucki, A. U. B. Wolter, H.-J. Grafe, B. Büchner, and C. Hess, Evolution of the nematic susceptibility in $\text{LaFe}_{1-x}\text{Co}_x\text{AsO}$, *Phys. Rev. Lett.* **125**, 067001 (2020).
- [42] C. Wuttke, F. Caglieris, S. Sykora, F. Steckel, X. Hong, S. Ran, S. Khim, R. Kappenberger, S. L. Bud'ko, P. C. Canfield, S. Wurmehl, S. Aswartham, B. Büchner, and C. Hess, Ubiquitous enhancement of nematic fluctuations across the phase diagram of iron based superconductors probed by the Nernst effect, *Npj Quantum Mater.* **7** (2022).
- [43] R. Küchler, T. Bauer, M. Brando, and F. Steglich, A compact and miniaturized high resolution capacitance dilatometer for measuring thermal expansion and magnetostriction, *Rev. Sci. Instrum.* **83**, 095102 (2012).
- [44] J. Werner, W. Hergett, M. Gertig, J. Park, C. Koo, and R. Klingeler, Anisotropy-governed competition of magnetic phases in the honeycomb quantum magnet $\text{Na}_3\text{Ni}_2\text{SbO}_6$ studied by dilatometry and high-frequency ESR, *Phys. Rev. B* **95**, 214414 (2017).
- [45] S. Spachmann, A. Elghandour, M. Frontzek, W. Löser, and R. Klingeler, Magnetoelastic coupling and phases in the skyrmion lattice magnet Gd_2PdSi_3 discovered by high-resolution dilatometry, *Phys. Rev. B* **103**, 184424 (2021).
- [46] A. E. Böhmer, P. Burger, F. Hardy, T. Wolf, P. Schweiss, R. Fromknecht, H. v. Löhneysen, C. Meingast, H. K. Mak, R. Lortz, S. Kasahara, T. Terashima, T. Shibauchi, and Y. Matsuda, Thermodynamic phase diagram, phase competition, and uniaxial pressure effects in BaFe_2As_2 studied by thermal expansion, *Physical Review B* **86**, 10.1103/physrevb.86.094521 (2012).
- [47] A. V. Kityk, V. P. Soprunyuk, A. Fuith, W. Schranz, and H. Warhanek, Low-frequency elastic properties of the incommensurate ferroelastic $[\text{N}(\text{CH}_3)_4]\text{CuCl}_4$, *Physical Review B* **53**, 6337–6344 (1996).
- [48] N. Qureshi, Y. Drees, J. Werner, S. Wurmehl, C. Hess, R. Klingeler, B. Büchner, M. T. Fernández-Díaz, and M. Braden, Crystal and magnetic structure of the oxypnictide superconductor LaFeAsO : A neutron-diffraction study, *Physical Review B* **82**, 10.1103/physrevb.82.184521 (2010).
- [49] L. Wang, S. Sauerland, F. Scaravaggi, R. Kappenberger, S. Aswartham, S. Wurmehl, A. Wolter, B. Büchner, and R. Klingeler, Nematicity and structure in $\text{LaFe}_{1-x}\text{Co}_x\text{AsO}$, *Journal of Magnetism and Magnetic Materials* **482**, 50–53 (2019).
- [50] F. Scaravaggi, S. Sauerland, L. Wang, R. Kappenberger, P. Lepucki, A. P. Dioguardi, X. Hong, F. Caglieris, C. Wuttke, C. Hess, H.-J. Grafe, S. Aswartham, S. Wurmehl, R. Klingeler, A. U. B. Wolter, and B. Büchner, Revisiting the phase diagram of $\text{LaFe}_{1-x}\text{Co}_x\text{AsO}$ in single crystals by thermodynamic methods, *Phys. Rev. B* **103**, 174506 (2021).
- [51] E. C. Blomberg, A. Kreyssig, M. A. Tanatar, R. M. Fernandes, M. G. Kim, A. Thaler, J. Schmalian, S. L. Bud'ko, P. C. Canfield, A. I. Goldman, and R. Prozorov, Effect of tensile stress on the in-plane resistivity anisotropy in BaFe_2As_2 , *Physical Review B* **85**, 10.1103/physrevb.85.144509 (2012).
- [52] C. Dhital, Z. Yamani, W. Tian, J. Zeretsky, A. S. Sefat, Z. Wang, R. J. Birgeneau, and S. D. Wilson, Effect of uniaxial strain on the structural and magnetic phase transitions in BaFe_2As_2 , *Physical Review Letters* **108**, 10.1103/physrevlett.108.087001 (2012).
- [53] J. Hu, C. Setty, and S. Kivelson, Pressure effects on magnetically driven electronic nematic states in iron pnictide superconductors, *Physical Review B* **85**, 10.1103/physrevb.85.100507 (2012).
- [54] L. Wang, M. He, F. Hardy, P. Adelman, T. Wolf, M. Merz, P. Schweiss, and C. Meingast, Large nematic susceptibility in the double-4 magnetic phase of $\text{Ba}_{1-x}\text{Na}_x\text{Fe}_2\text{As}_2$, *Physical Review B* **97**, 10.1103/physrevb.97.224518 (2018).
- [55] W. Schranz, H. Kabelka, A. Sarras, and M. Burock, Giant domain wall response of highly twinned ferroelastic materials, *Applied Physics Letters* **101**, 10.1063/1.4757992 (2012).
- [56] Y. P. Varshni, Temperature dependence of the elastic constants, *Physical Review B* **2**, 3952–3958 (1970).
- [57] S. Aswartham, C. Nacke, G. Friemel, N. Leps, S. Wurmehl, N. Wizen, C. Hess, R. Klingeler, G. Behr, S. Singh, and B. Büchner, Single crystal growth and physical properties of superconducting ferro-pnictides $\text{Ba}(\text{Fe,Co})_2\text{As}_2$ grown using self-flux and Bridgman techniques, *Journal of Crystal Growth* **314**, 341–348 (2011).
- [58] N. Ni, A. Thaler, A. Kracher, J. Q. Yan, S. L. Bud'ko, and P. C. Canfield, Phase diagrams of BaFe_2As_2 single crystals, *Physical Review B* **80**, 10.1103/physrevb.80.024511 (2009).
- [59] R. M. Fernandes, E. Abrahams, and J. Schmalian, Anisotropic in-plane resistivity in the nematic phase of the iron pnictides, *Physical Review Letters* **107**, 10.1103/physrevlett.107.217002 (2011).
- [60] M. Breitzkreiz, P. M. R. Brydon, and C. Timm, Resistive anisotropy due to spin-fluctuation scattering in the nematic phase

- of iron pnictides, *Physical Review B* **90**, 10.1103/physrevb.90.121104 (2014).
- [61] M. N. Gastiasoro, P. J. Hirschfeld, and B. M. Andersen, Origin of electronic dimers in the spin-density wave phase of Fe-based superconductors, *Physical Review B* **89**, 10.1103/physrevb.89.100502 (2014).
- [62] M. N. Gastiasoro, I. Paul, Y. Wang, P. Hirschfeld, and B. M. Andersen, Emergent defect states as a source of resistivity anisotropy in the nematic phase of iron pnictides, *Physical Review Letters* **113**, 10.1103/physrevlett.113.127001 (2014).
- [63] M. P. Allan, T.-M. Chuang, F. Masee, Y. Xie, N. Ni, S. L. Bud'ko, G. S. Boebinger, Q. Wang, D. S. Dessau, P. C. Canfield, M. S. Golden, and J. C. Davis, Anisotropic impurity states, quasiparticle scattering and nematic transport in underdoped $\text{Ca}(\text{Fe}_{1-x}\text{Co}_x)_2\text{As}_2$, *Nature Physics* **9**, 220–224 (2013).
- [64] S. Ishida, M. Nakajima, T. Liang, K. Kihou, C. H. Lee, A. Iyo, H. Eisaki, T. Kakeshita, Y. Tomioka, T. Ito, and S. Uchida, Anisotropy of the in-plane resistivity of underdoped BaFe_2As_2 superconductors induced by impurity scattering in the antiferromagnetic orthorhombic phase, *Physical Review Letters* **110**, 10.1103/physrevlett.110.207001 (2013).
- [65] H.-H. Kuo and I. R. Fisher, Effect of disorder on the resistivity anisotropy near the electronic nematic phase transition in pure and electron-doped BaFe_2As_2 , *Physical Review Letters* **112**, 10.1103/physrevlett.112.227001 (2014).
- [66] M. N. Gastiasoro, *Emergent disorder phenomena in correlated Fe-based superconductors*, Ph.D. thesis, University of Copenhagen (2016).
- [67] F. Hammerath, P. Bonfà, S. Sanna, G. Prando, R. De Renzi, Y. Kobayashi, M. Sato, and P. Carretta, Poisoning effect of Mn in $\text{LaFe}_{1-x}\text{Mn}_x\text{AsO}_{0.89}\text{F}_{0.11}$: Unveiling a quantum critical point in the phase diagram of iron-based superconductors, *Physical Review B* **89**, 10.1103/physrevb.89.134503 (2014).
- [68] M. Moroni, S. Sanna, G. Lamura, T. Shiroka, R. De Renzi, R. Kappenberger, M. A. Afrassa, S. Wurmehl, A. U. B. Wolter, B. Büchner, and P. Carretta, Competing effects of Mn and Y doping on the low-energy excitations and phase diagram of $\text{La}_{1-y}\text{Y}_y\text{Fe}_{1-x}\text{Mn}_x\text{AsO}_{0.89}\text{F}_{0.11}$ iron-based superconductors, *Physical Review B* **94**, 10.1103/physrevb.94.054508 (2016).
- [69] M. Moroni, P. Carretta, G. Allodi, R. De Renzi, M. N. Gastiasoro, B. M. Andersen, P. Materne, H.-H. Klauss, Y. Kobayashi, M. Sato, and S. Sanna, Fast recovery of the stripe magnetic order by Mn/Fe substitution in F-doped LaFeAsO superconductors, *Physical Review B* **95**, 10.1103/physrevb.95.180501 (2017).
- [70] M. N. Gastiasoro, F. Bernardini, and B. M. Andersen, Unconventional disorder effects in correlated superconductors, *Physical Review Letters* **117**, 10.1103/physrevlett.117.257002 (2016).
- [71] G. Wu, H. Chen, Y. L. Xie, Y. J. Yan, T. Wu, R. H. Liu, X. F. Wang, D. F. Fang, J. J. Ying, and X. H. Chen, Superconductivity induced by oxygen deficiency $\text{La}_{0.85}\text{Sr}_{0.15}\text{FeAsO}_{1-\delta}$, *Physical Review B* **78**, 10.1103/physrevb.78.092503 (2008).